Nanocrystalline $NiWO_4$-WO_3-$WO_{2.9}$ Composite strings: Fabrication, Characterization and their Electrocatalytic Performance for Hydrogen Evolution Reaction

Shaheen Fatima Anis[1], Ahmad O. Mostafa[2], Nidal Hilal[1,3], Raed Hashaikeh[1,*]

[1] NYUAD Water Research Center, Engineering Division, New York University Abu Dhabi, Abu Dhabi, Postal code 00000. United Arab Emirates.

[2] Department of Mechanical Engineering, Tafila Technical University, Tafila 66110, Jordan.

[3] Centre for Water Advanced Technologies and Environmental Research (CWATER), College of Engineering, Swansea University, Fabian Way, Swansea SA1 8EN. United Kingdom.

*Corresponding author: raed.hashaikeh@nyu.edu

Abstract

In this study, novel nano crystalline composite strings made from mixed nickel-tungsten oxides ($NiWO_4$-WO_3-$WO_{2.9}$) have been fabricated. The NiWO4-WO_3 fibers produced by the electrospinning method were post treated in an argon atmosphere at 800°C which yielded $NiWO_4$-WO_3-$WO_{2.9}$ nanocrystals attached together forming a string-like structure. The presence of $WO_{2.9}$ phase was confirmed by both the XRD and TEM diffraction pattern analysis. String morphology and structure were found to change with different post treatment conditions such as by changing the calcination temperature from 550°C under oxygen to 800°C under pure argon atmosphere. This material was investigated for electrocatalytic hydrogen evolution reaction (HER) in 0.5 M H_2SO_4 and 0.1M KOH electrolytes. These composite strings showed good electrocatalytic activity compared to the $NiWO_4$-WO_3 fibers reported previously [1]. It was concluded that the presence of $WO_{2.9}$ phase increases the electrocatalytic activity of the catalyst as compared to the $NiWO_4$-WO_3 fibers with over potentials as low as 40 mV and 50 mV in 0.5 M H_2SO_4 and 0.1M KOH respectively.

Keywords: Electrospinning, nickel tungstate, tungsten oxide, composite strings, hydrogen evolution reaction.

1. Introduction

In an effort to address the growing global energy demands, the quest for efficient electrocatalysts still continues, with new materials being investigated for hydrogen evolution reaction (HER) [2-6]. Hydrogen is a promising alternative to fossil fuels due to the numerous advantages it offers such as being pollution-free and sustainable [7]. Moreover, hydrogen production through water electrolysis has attracted much interest as hydrogen can be produced in high purity and large quantities [8]. At the same time, the generated gases from water electrolysis have proved useful in other applications such as self-cleaning membranes [9-11]. Several metal oxide electrocatalysts have been put forward for HER including NiO [12], WO_3 [13], ZnO [14] and MoO [15]. Nevertheless, the methods of producing catalytic fibers, nanorods, nanowires or string-like structures are gaining importance in recent literature studies [16]. Among these methods, electrospinning has stood out to be a versatile, flexible and cost effective method for metal oxide fibrous production. In electrospinning, a syringe is filled with the desired solution. The needle of the syringe is connected to a collector via high voltage. The electrical charge draws very fine fibers from the needle tip, which gets accumulated on the collector [17, 18]. Fabrication of metal oxide fiber like structures through the electrospinning method has attracted much interest, where it is being studied in various applications such as WO_3 fibers for gas sensing [19], NiO nanorods [20] and $TiNb_2O_7$ strings [21] for batteries, TiO_2 fibers for hydrogenation [22] and ZnO nanofibers for photocatalysis [23]. However, the research on fibrous electrocatalysts is still an emerging area with only few studies reported on the fabrication, characterization and application on electrocatalyst fibers for HER. Recently, Wang et al. [24] reported low Tafel slopes of about 34 mV/dec for $CoSe_2$ nanowires grown on carbon fiber paper. Chekin et al. [25] reported enhanced electrocatalytic activity of WO_3 nanorods when used in conjunction with carbon nanotubes (CNTs). A current density of 3.8 mA/cm^2 was reported as compared to commercial WO_3 particles registering a current density of 0.8 mA/cm^2 at a potential of -0.8 V. They also observed a low Tafel slope of 104 mV/dec for WO_3 nanorods compared to 130 mV/dec for WO_3 particles. The use of CNTs along with the electrocatalytic material may be attributed to CNTs superior catalytic

properties owing to its high electrical conductivity and better electron transport characteristics [26, 27].

The electrospinning process offers an advantage of producing mixed oxides in the end morphology structures [28, 29]. The electrospinning solution can be tailored to incorporate a combination of different elemental salts. Several oxide mixtures including Ti-based mixed oxide fibers [29], ZnO-NiO hybrid fibers [30] and ZnO-SnO_2 mixed oxide fibers [31] have been reported. Wu et al. [32] reported a Tafel slope of 89 mV/dec in 0.5M H_2SO_4 electrolyte using electrospun $MnCo_2O_4$ fibers when tested for HER. Recently, our group reported the fabrication of electrospun mixed oxides WO_3-$NiWO_4$ and $NiWO_4$-WO_3-NiO composite fibers for HER, where fibers with different compositions were produced by varying the electrospinning solution parameters [1] . The presence of $NiWO_4$ phase in WO_3- $NiWO_4$ fibers enhanced the electrocatalytic activity for HER when compared with pure WO_3 and NiO fibers. Low overpotentials of 80 mV and 60 mV in 0.5M H_2SO_4 and 0.1 KOH media respectively were reported. The composite fibers also registered low Tafel slopes of 50.2 mV/dec and 41.9 mV/dec in 0.5M H_2SO_4 and 0.1 KOH media respectively.

With the ongoing efforts to find promising electrocatalysts, $WO_{2.9}$ phase is reported to be potential candidate [33]. The fabrication of $WO_{2.9}$ phase has been reported in a few studies. Al-Sharab et al. [34] synthesized $WO_{2.9}$ fibers by evaporating WO_3 powder in a transmission electron microscope (TEM) chamber using the electron beam. The same phase was synthesized [34] under an inert gas condensation system, whereby the WO_3 powder was evaporated in a reduced pressure chamber in the presence of an argon gas. Xu et al. [35] synthesized aligned $WO_{2.9}$ fibers via flame synthesis method utilizing a tungsten substrate. Li et al. [33] synthesized $WO_{2.9}$ nanoparticles by annealing ball milled commercial WO_3 particles in a tube furnace for one hour under H_2-Ar atmosphere. They [33] also tested electrocatalytic activity for HER in 0.5M H_2SO_4 where the $WO_{2.9}$ nanoparticles registered a low Tafel slope of 50 mV/dec and an overpotential of 70 mV.

This study aims at fabricating $NiWO_4$-WO_3-$WO_{2.9}$ composites in the string morphology using the electrospinning method. Moreover, it is an effort to further improve the previously reported [1]

$NiWO_4$-WO_3 composite fibers for HER. To the best of our knowledge, no study on the direct synthesis of this combination of composite fibers could be found in the literature.

2. Materials and Methods

2.1 Materials

The following salts, solvents, polymer, and acids were obtained from Sigma-Aldrich: nickel II acetate (NiAc), ammonium metatungstate hydrate (AMT), ethanol (≥ 99%), polyvinylpyrrolidone (PVP, Mw = 1,300,000), sulfuric acid (>90%) and potassium hydroxide (KOH). The salts, polymer and solvents were used in their as-received form, while the acids were adjusted to their required compositions. CNS was developed by Applied Nanostructured Solutions, LLC through a continuous chemical vapor deposition process [36].

2.2 Fabrication of Mixed Nickel-Tungsten Oxide Nanocrystalline Strings

Mixed $NiWO_4$-WO_3 composite fibers were prepared by the electrospinning method. A Nanon-01A electrospinning setup (MECC, Japan) was used for this purpose. $NiWO_4$-WO_3 electrospun fibers were produced by following the method reported earlier by Anis et al. [1]. NiAc and AMT salts were first dissolved in deionized (DI) water. A clear salt solution was obtained. Following this, PVP was added to facilitate the electrospinning process [37] by increasing the electrospinning solution viscosity. The molar ratio of Ni: W was kept as 1:2. Electrospinning was carried out using a stainless steel needle of gauge 22 at a 0.5 ml/h flow rate and 28 kV voltage. The as-spun fibers were allowed to dry at 80°C for 6 h, after which they were calcined at 550°C for 2 h. calcination was carried out to remove the PVP polymer and produce pure mixed metal oxide fibers. For convenience, specimens prepared by mixing $NiWO_4$-WO_3 composite with Ni: W of 1:2 molar ratios are designated as NW12. The NW12 fibers, after calcination at 550°C, were further treated at 800°C under a pure argon atmosphere in a tube furnace for 60 minutes. The pressure inside the tube was maintained at 0.03 MPa. The resulting fibrous material was collected after the tube furnace cooling down to room temperature. The specimen processed under these conditions is designated as NW12-Ar throughout the manuscript referring to NW12

fibers treated in argon atmosphere. Another as-spun specimen was heat treated directly at 800°C in air, without calcination at 550°C, to compare their electrocatalytic activity with the other catalytic fibers fabricated in this study. This specimen is designated as NW12-O. The symbol O signifies the presence of oxygen.

2.3 Mixed Nickel-Tungsten Oxide Nanocrystalline String Characterization

Nova Nano Scanning electron microscopy (high resolution SEM, FEI) operating at 10 kV and a high resolution transmission electron microscope (HRTEM) (Tecnai F20, FEI), operating at 200kV were used to study the mixed metal oxide fiber morphology. SEM energy dispersive X-ray (EDS) detector was used for elemental analysis. For SEM analysis, the fibers were directly deposited onto the SEM stub, while for TEM, the sample was sonicated for 15 minutes before deposition on a copper grid. Structural analysis was performed through an X-ray diffractometer (PANalytical, Emperean). Ni-filtered CuKα (λ= 1.5056 Å) radiations were used in the range of 10-90° 2θ, with 45 kV and 40 mA voltage and current.

2.4 Electrochemical Characterization

The catalytic composite strings were dispersed in ethanol, after which carbon nano structures (CNS) was added and dispersed through sonication using a BRANSON 1510 model until a uniform suspension was obtained. Metal oxide electrocatalysts are often used in conjunction with CNTs or CNS for superior catalytic properties due to their high electrical conductivity and better electron transport [26, 27]. Fiber to CNS ratio (by weight) was kept as 80:20. To prepare the working electrode, a clean glassy carbon electrode (GCE) was coated with a fixed volume of the suspension by the drop casting. A mass loading of 0.1 mg/cm^2 catalyst was used in this study. Following this, the electrode was further dried in an oven at 50°C for 30 minutes.

The metal oxide composite string was tested as an electrocatalyst for HER in acidic and alkaline media as $H3O^+$ and OH^- are two of the most conductive ions [38]. A three-electrode system was

used [1] to test the electrocatalytic performance of NW12, NW12-O and NW12-Ar strings in 0.5M H_2SO_4 and 0.1M KOH solutions. This was performed using an Autolab302N potentiostat/galvanostat, where linear polarization (LP) graphs were obtained at a scan rate of 50mV/s. The reference and counter electrode were Ag|AgCl|KCl3.5M and a platinum wire respectively. The potentials are reported with reference to a reversible hydrogen electrode (RHE).

3. Results

3.1 Structural and Morphological Characterization of the Mixed Metal Oxides

The experimental XRD patterns were analyzed in X'pert Highscore software using Rietveld refinement [39]. Standard patterns for the expected phases were acquired from Pearson's Crystal Structure Database for Inorganic Compounds [40] and used for phase identification. Figure 1 shows the XRD patterns of NW12, NW12-O and NW12-Ar samples. The peaks of both $NiWO_4$ (monoclinic structure, $MgWO_4$ prototype, *P12/c1* space group and 13 space group number with *a*=4.599Å, *b*=5.669Å and *c*=4.913Å lattice parameters) and room temperature WO_3 (triclinic structure, WO_3 prototype, *P-1* space group and 2 space group number with *a*=7.375Å, *b*=7.507Å and *c*=7.710Å lattice parameters) compounds could be positively identified in all samples. However, the pattern of the annealed sample at 800°C under argon (NW12-Ar) showed few differences than other two patterns. The difference was due to the presence of $WO_{2.9}$ compound, which is believed to have monoclinic structure, $WO_{2.9}$ prototype, *P12/m1* space group and 10 space group number with *a*=7.316Å, *b*=7.534Å and *c*=10.557Å lattice parameters. Detailed crystallographic data of the identified phases in all samples are provided in Table 1. The XRD pattern refinement for NW12-Ar sample was challenging, because many of WO_3 and $WO_{2.9}$ peaks were found overlapping. Nevertheless, the phase identification in this work was successful and conforms with the O-W binary phase diagram [41] data.

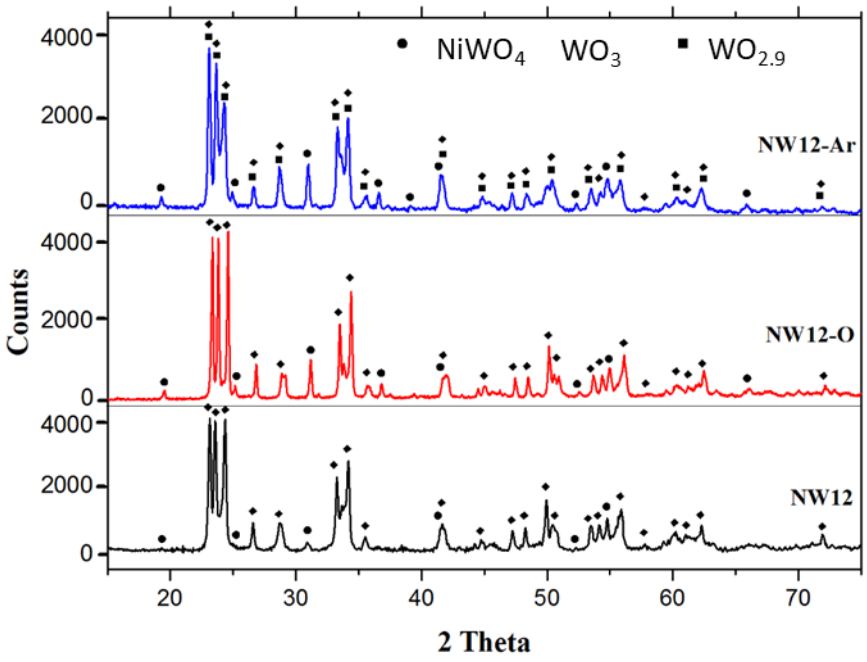

Figure 1: XRD patterns of NW12, NW12-O and NW12-Ar samples

Table 1: Crystallographic data of the detected phases in the current study

Phase	Crystallographic system	Prototype	Space group	Lattice parameters (Å)			Angles (°)		
				a	*b*	*c*	*α*	*B*	*γ*
WO_3	Triclinic	WO_3	*P-1*	7.375	7.507	7.710	89.97	89.63	89.86
$WO_{2.9}$	Monoclinic	$WO_{2.9}$	*P12/m1*	7.316	7.534	10.557		133.19	
$NiWO_4$	Monoclinic	$MgWO_4$	*P12/C1*	4.599	5.669	4.913		89.94	

Figure 2 shows the O-W binary phase diagram in a condensed system at 0.1 MPa [41]. Several compounds exist in a very narrow composition range (73-75 at. % O). These compounds are $W_{18}O_{49}$, $W_{24}O_{68}$, W_nO_{3n-2} series, W_nO_{3n-1} series and WO_3. Therefore, any deviation in oxygen composition below 75 at. % will lead to different phase formation. For instance, NW12-Ar and NW12-O samples were both annealed at 800°C in argon and oxygen atmospheres, respectively.

The phase content of NW12-Ar was maintained as $NiWO_4$, WO_3 and $WO_{2.9}$, while the oxygen concentration increased upon annealing and thus WO_3 grew on the expense of $WO_{2.9}$ to have only WO_3 and $NiWO_4$ in NW12-O sample. In principle, both $WO_{2.9}$ and WO_3 phases exist as stoichiometric compositions. Figure 3 is drawn to describe the crystal structure and diffraction pattern of these two compounds.

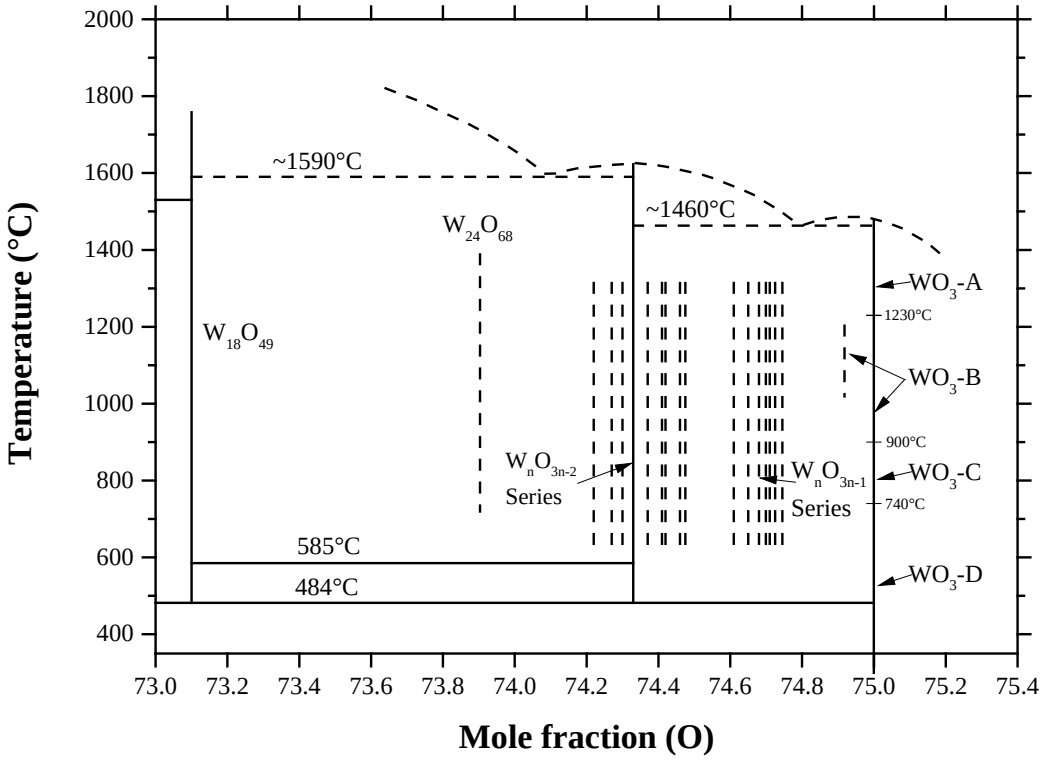

Figure 2: The O-W binary phase diagram in a condensed condition at 0.1 MPa.

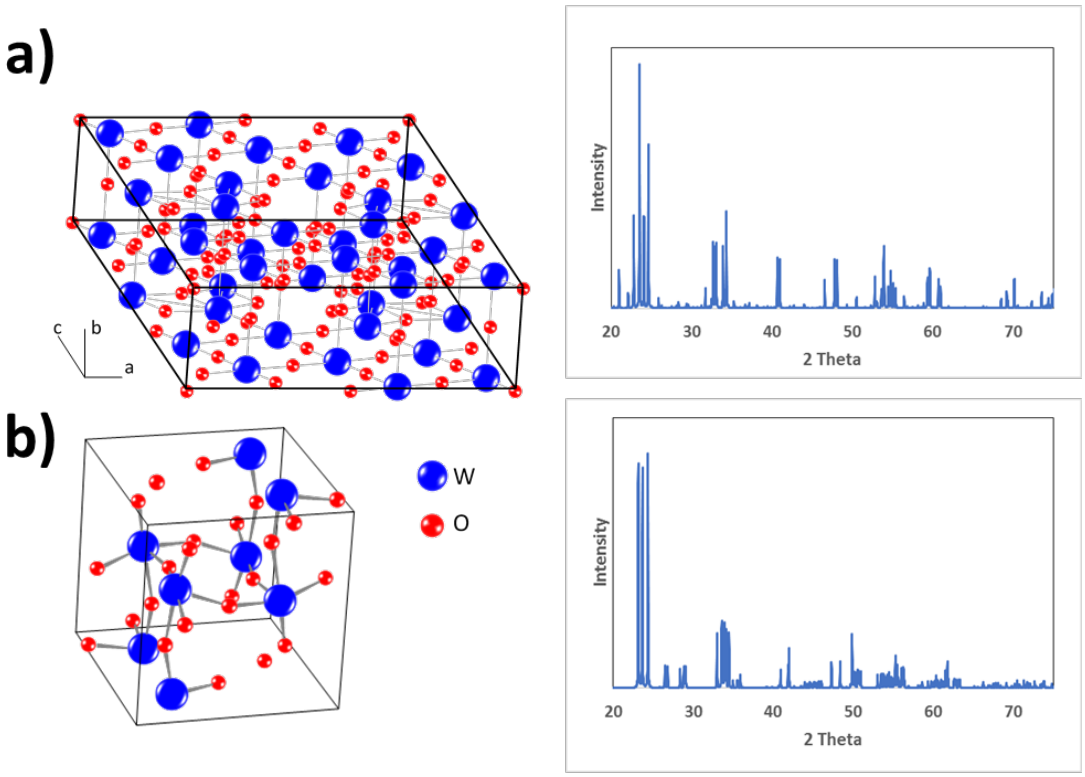

Figure 3: Unit cells and standard XRD patterns of (a) $WO_{2.9}$ and (b) WO_3.

In order to calculate the relative amounts of all detected phases, Rietveld refinement [39] was performed, which is based on the best fit with the measured patterns using a least square approach. The bar chart in Figure 4 summarizes the relative amounts of the detected phases by XRD analysis. Details on the fitting procedure are included in the supplementary information.

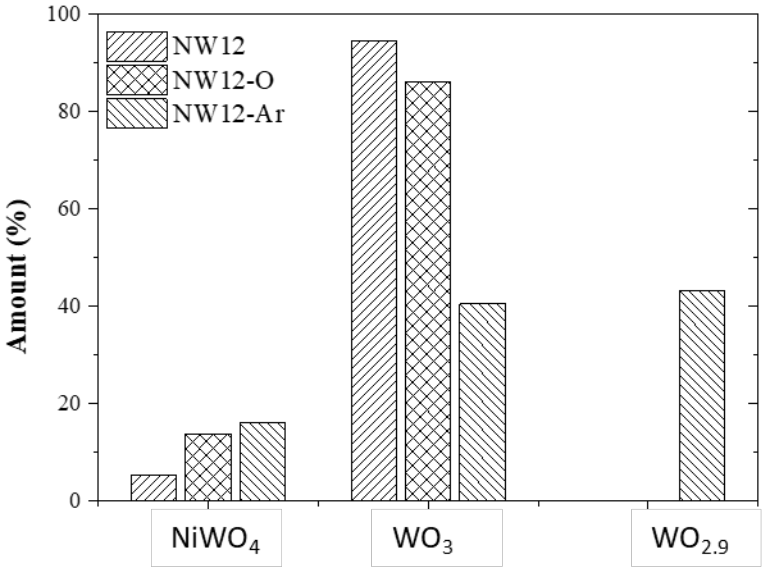

Figure 4: Bar chart represents the relative amounts of detected phases for NW12, NW12-O and NW12-Ar specimens.

The amount of $NiWO_4$ was relatively high (16.1%) in NW12-Ar as compared to 5.3 and 13.8% in NW12 and NW12-O, respectively. While, WO_3 was dominant in NW12 sample due to the reasons discussed in a previous study published by Anis et al. [1]. The amounts of WO_3 and $WO_{2.9}$ were about 40.6% and 43.3%, respectively, in NW12-Ar. The approach of treating O-W samples under various atmospheres including hydrogen [33] and argon [34] has been reported, whereby $WO_{2.9}$ phase was obtained. However, different atmospheric variations including the gas type and pressure maintained in the tube chamber might produce phases with different compositions. Hence, this opens new research areas to further study the effect of different conditions on $WO_{2.9}$ phase formation.

Figure 5 shows the HR-SEM images of NW12, NW12-O and NW12-Ar. Fiber like morphology was observed for NW12 (Figure 5a), similar to the one reported in [1]. Large tungsten crystals can be observed along the fiber, while the fiber itself is made from tiny particles composed of both $NiWO_4$ and WO_3 [42]. A change in composite fiber morphology occurred when the as-spun fibers were treated at 800°C in air instead of 550°C. The morphology of the fibers changed from fibrous to more like 'strings' as shown in Figure 5b. Larger crystals compared to NW12 were observed in this case. The high temperature provided the driving force for the small crystals to grow through

241 the diffusion process [42]. When the NW12 fibers were treated at 800°C under an argon
242 atmosphere, again a 'string-like' morphology was observed. The nanocrystals can be seen to be
243 attached together to form a string in Figure 5c. These morphological differences are attributed
244 to the different phase contents as concluded from the XRD analysis. Figure 6 shows the SEM
245 image of NW12-Ar and their corresponding EDS spectrums. Figure 6a shows the EDS spectrum
246 corresponding to the spot location on a single crystal, while Figure 6b shows the spectrum
247 corresponding to a spot along the fiber in NW12-Ar sample. EDS analyses revealed that the fibers
248 consist of Ni, W and O, while the pure tungsten oxide crystal consists of only W and O elements.
249 The small Ni signals are due to the presence of $NiWO_4$ phase along the string. The copper peak
250 corresponds to the copper tape on which the material was placed, while the Al peak corresponds
251 to the Al stub used during the SEM analysis.

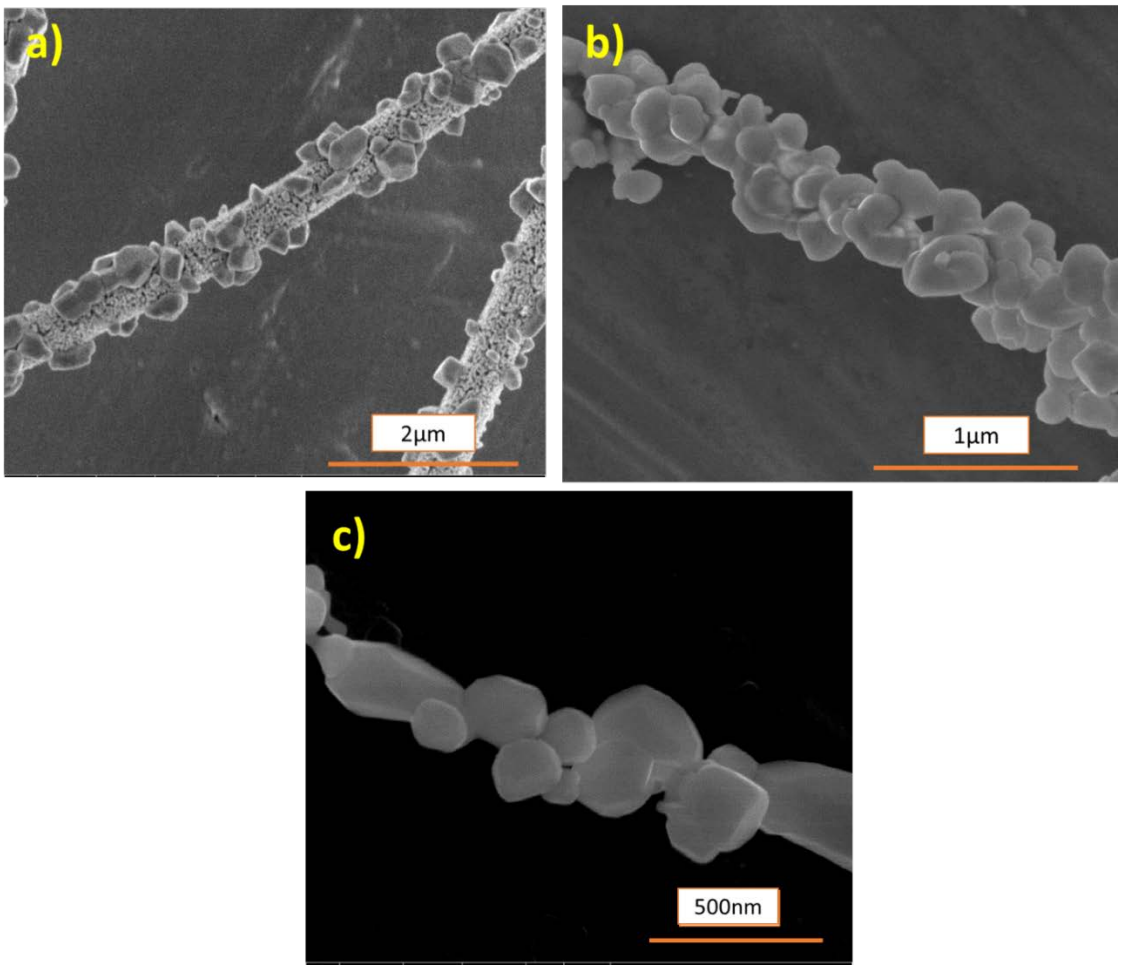

252

253 Figure 5: HR-SEM images of (a) NW12, (b) NW12-O and (c) NW12-Ar.

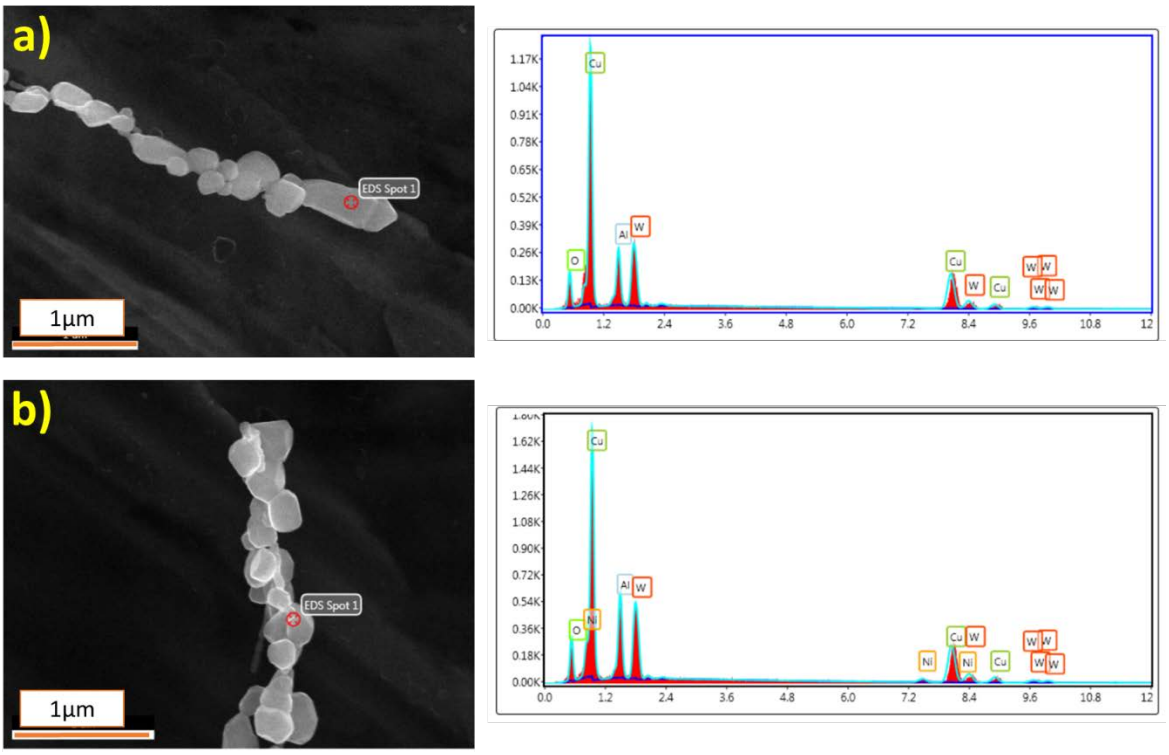

Figure 6: HRSEM images for NW12-AR and their corresponding EDS spectrums. The spectrum particularly corresponds to the EDS spots shown in the SEM images (a) at the single crystal and (b) along the string with a few crystals overlapping.

Both SEM and TEM provided valuable structural and compositional information for the composite strings. While SEM gave us an indication of the overall fiber morphology, owing to bulk EDS analysis, it was not possible to conclude the precise location of the phases in the composite string. Thus, TEM was use for this purpose. Figure 7 shows TEM images of NW12, NW12-O and NW12-Ar. The TEM images provide greater insight on fiber morphology, which are indeed made from crystals of different sizes depending upon their post treatment procedures. Figure 7a shows the morphology of $NiWO_4$-WO_3 composite fibers with Ni: W molar ratio of 1:2. The fiber is seen to be made from very small particles which are essentially much smaller than 10nm in size. However, when the same as-spun fibers were calcined at 800°C, larger crystals are observed (Figure 7b) on the expense of the smaller ones. Clearly, crystal growth has occurred. Similar is observed for the NW12-Ar (Figures 7c and 7d) which are composed of large crystals. String morphology does not change much when the NW12 fibers are post treated in either Argon

271 at 800°C or directly annealed at 800°C in air. The SAED spot pattern in Figure 7d corresponds to
272 the WO2.9 phase indicating the monoclinic symmetry (space group *P12/m1*) with lattice
273 parameters *a*=7.316 Å, *b*=7.534 Å, *c*=10.557 Å and β=133.19°. The selected area diffraction
274 (SAED) pattern of $WO_{2.9}$ has been coincided with another pattern from adjacent crystals. The
275 planes labelled in the inset are (1 1 1), (3 1 1) and (4 0 0) corresponding to d-spacings of 3.11 Å,
276 1.48 Å and 1.33 Å, respectively.

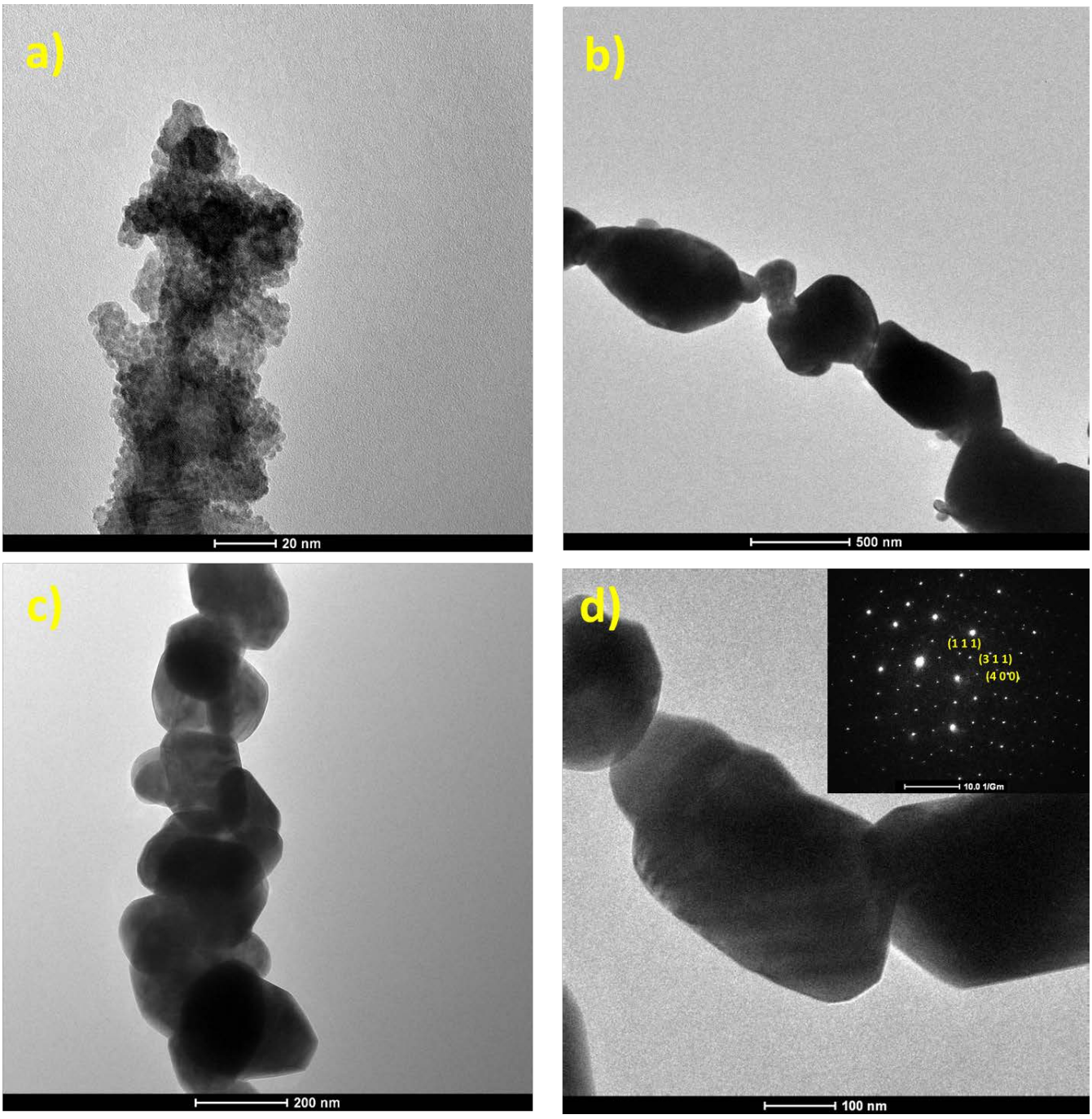

Figure 7: HR-TEM images of (a) NW12, (b) NW12-O and (c) NW12-Ar (d) NW12-Ar string along with corresponding SAED pattern in inset.

3.2 Electrocatalytic Activity of the Mixed Metal Oxides in Acidic and Alkaline Media

NW12-Ar and NW12-O were studied for their hydrogen evolution electrocatalytic properties in both acidic and alkaline media. Their electrocatalytic properties have been compared with pristine NiO and WO_3 fibers for comparison, as well as with NW12 to study the effect of $WO_{2.9}$ phase on HER. NW12-O was tested to confirm the reason for the enhanced electrocatalytic performance, whether due the presence of $WO_{2.9}$ or the large amount of $NiWO_4$ phase (≈16 %) in the nanocrystalline string. All over-potentials for hydrogen evolution were measured at a current density of -1 mA/cm^2 in both 0.5 M H_2SO_4 and 0.1M KOH media unless otherwise stated. The GCE shows negligible electrocatalytic activity as already established in the literature with high over potentials greater than 500mV [1, 25]. Therefore, any electrocatalytic activity is from the material fiber or string indeed.

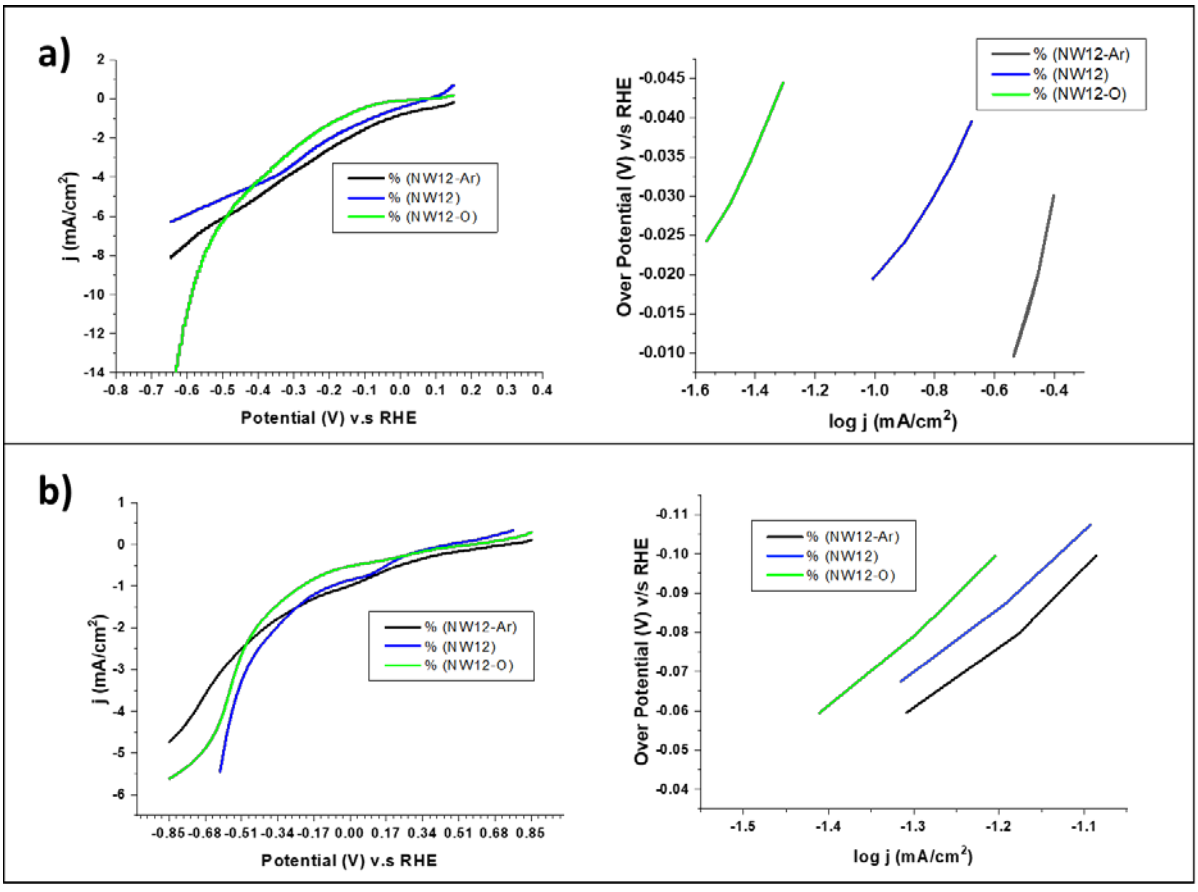

Figure 8: Polarization curves and their corresponding Tafel slopes for NW12-Ar, NW12 and NW12-O in (a) 0.5M H_2SO_4 and (b) 0.1M KOH.

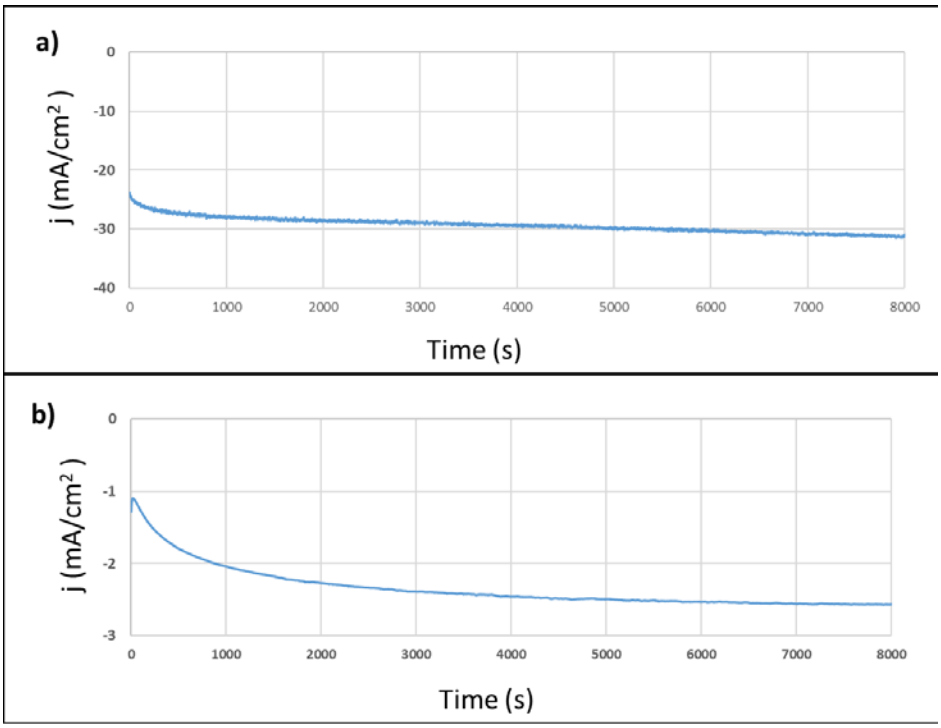

Figure 9: catalyst stability over time - chronoamperometric response curves of NW12-Ar at a constant overpotential of -150 mV for HER in a 0.5 M H2SO4 and b 0.1 M KOH.

Linear polarization (LP) curves for NW12-Ar, NW12 and NW12-O are compared in Figure 8. Figure 8a compares the LP curves and Tafel plots for HER in 0.5 M H_2SO_4 while Figure 8b compares it in 0.1M KOH. Table 2 summarizes the Tafel slopes and over potentials for the composite metal oxides in this study and compares it with pristine WO_3 and NiO fibers carried out in a previous study [1]. The highest Tafel slopes are reported for NiO in both electrolytes while low Tafel slopes are registered for the composite fibers, especially for NW12-Ar. Figure 9 shows the catalyst strings, NW12-Ar stability in both 0.5 M H_2SO_4 and 0.1 M.

4. Discussion

Thus far, the most promising electrocatalyst for hydrogen evolution reported in the literature is platinum [38] with very low over potentials observed in both acidic and alkaline media of about 10mV [1, 43]. This makes platinum the most valued material for HER at present. Table 2

compared the over potentials and Tafel slopes for NW12, NW12-O, NW12-Ar, pure WO_3 and NiO electrospun fibers. NiO was found to have poor electrocatalytic properties on its own. WO_3 also registered high over potential and Tafel slope as compared to the composite fibers.

Interestingly, there is a correlation between the morphology and composition of the fibers to their electrocatalytic activity. On comparing the NW12 fibers to the NW12-O strings, at first it can be expected that NW12-O may perform better due to higher percentage of $NiWO_4$ phase (≈14 wt. %) as opposed to just about 5 wt. % in NW12 fibers. This anticipation is due to the fact that the presence of $NiWO_4$ phase along with WO_3 has already been proven to be beneficial for HER [1]. However, large over potentials are registered for NW12-O, 220 mV and 240 mV in acidic and alkaline media respectively. The over potential for NW12-O in 0.5M H_2SO_4 is in fact greater than that reported for pristine WO_3 fibers. A possible explanation for this is the morphology of NW12-O. At high temperatures, the crystal size increases and the fiber morphology changes to a string made from randomly shaped particles as could be seen in Figures 5 and 7. This can be attributed to a higher calcination temperature of 800^oC used for the as-spun fibers. The NW12 over potentials (82mV and 60mV in 0.5M H_2SO_4 and 0.1M KOH respectively) and Tafel slopes (55.0 mV/dec and 39.9 mV/dec in 0.5M H_2SO_4 and 0.1M KOH respectively) reported in this work are quite similar to the ones previously reported in [1]. This is due to a similar electrochemical setup, together with similar mass loadings used.

An over potential of 40mV is observed for NW12-Ar. This is much lower compared to the over potential for NW12-O, signifying the presence of $WO_{2.9}$ phase in the fiber which is stipulated to play a critical role in the electrocatalytic activity for HER. Likewise, a low over potential of 50 mV is registered for NW12-Ar in 0.1M KOH electrolyte compared to 60 mV for NW12. However, a greater Tafel slope of 45 mV/dec is observed for NW12-Ar compared to 39.9 mV/dec for NW12 fibers. Nevertheless, there is not a significant difference between the two values. It should be noted that different values of overpotentials and Tafel slopes are registered for the same material in the two different electrolytes due to the difference in kinetics [1, 13].

Literature studies reported over potentials and Tafel slopes of various electrocatalysts in different electrolyte media with different mass loadings [44, 45]. Hence, a direct comparison with

the literature data becomes difficult due to overall different working cell conditions and electrode preparations. In this study, 0.1 mg/cm^2 mass loading for the catalyst was used, which was similar to the one in our previous reported study [1] on mixed nickel-tungsten oxide and pure WO_3 and NiO electrospun fibers for HER in 0.5M H_2SO_4 and 0.1M KOH. Mass loading of catalyst indeed plays a crucial role as a higher mass loading usually leads to greater current [12]. The $WO_{2.9}$ nano particles for HER in acidic media [33] gave an over potential of 70 mV and a Tafel slope of 50 mV/dec with a mass loading of 0.285 mg/cm^2. Many of the phosphide electrocatalysts such as FeP [46] and CoP [47] have also reported to register low over potentials. For example, CoP nanowires gave an overpotential of about 38mV and a Tafel slope of 51 mV/dec in acidic media. However, the mass loading utilized was 0.92 mg/cm^2. Similarly, FeP nanoparticles [46] gave overpotential of 55 mV in acidic media with a mass loading of 3.2 mg/cm^2 which is quite higher than the one reported in this study. The low over potentials and Tafel slopes of NW12-Ar fibers in both acidic and alkaline media attests to its potential for HER activity.

NW12-Ar also have good stability under longer times in both acidic and alkaline media, as shown in Figure 9. Under an overpotential of 150 mV, the current density of the catalyst was seen to increase initially with time, after which it maintained a constant value at -30 mA/cm^2 and -2.6 mA/cm^2 in 0.5M H_2SO_4 and 0.1M KOH respectively. The initial increase in current density is attributed to the time dependent wetting of CNS, where the initial hydrobhobicity of CNS, decreases from 105^o to 0^o in 15 minutes [10].

The current study provides a further insight on mixed oxide fibrous materials and their change in morphology upon post treatment, which is still limited in literature. Furthermore, it paves way for synthesizing composite strings with the simple electrospinning technique whereby simple post treatment steps can produce different compositions. Lastly, NW12-Ar can be further explored for their potential applications besides electrocatalysis, such as in photoelectrochemical reactions, similar to the way NW12 fibers were tested [42].

Table 2: Comparison of electrocatalytic parameters for NW12-Ar, NW12 and NW12-O.

Material	0.5M H2SO4		Reference
	Over potential (mV)	Tafel Slope (mV/dec)	
NW12	82	55.0	This work
NW12-O	220	70.1	This work
NW12-Ar	40	69.0	This work
WO_3	150	140.5	[1]
NiO	480	269.6	[1]
	0.1M KOH		
	Over potential (mV)	Tafel Slope (mV/dec)	
NW12	60	39.9	This work
NW12-O	240	128.2	This work
NW12-Ar	50	45.0	This work
WO_3	270	134.8	[1]
NiO	410	258.4	[1]

5. Conclusion

Post treatment of electrospun WO_3- $NiWO_4$ fibers in an inert atmosphere at 800°C, produced WO_3-$NiWO_4$-$WO_{2.9}$ composite strings. Morphology and structural characteristics were studied through various techniques. The change in morphology and composition brought about a change in the electrocatalytic properties of the nanocrystalline string altogether. When tested for HER, WO_3- $NiWO_4$-$WO_{2.9}$ strings gave a low over potential in both acidic and alkaline media. The presence of $WO_{2.9}$ phase was responsible for this improvement which was further confirmed by testing the as spun WO_3- $NiWO_4$ fibers calcined directly at 800^oC under air. The fibers calcined at

800°C under air produced a higher percentage of $NiWO_4$ phase but it failed to register promising electrocatalytic activity, hence attesting that $WO_{2.9}$ indeed plays a crucial electrocatalytic role.

Acknowledgement

The authors would like to thank Florent Ravaux, Masdar Institute, Khalifa University of Science and Technology for extending his help during TEM.

Funding

This research did not receive any specific grant from funding agencies in the public, commercial, or not-for-profit sectors

Conflicts of Interest

None.

References

[1] S.F. Anis, B.S. Lalia, A.O. Mostafa, R. Hashaikeh, Electrospun nickel–tungsten oxide composite fibers as active electrocatalysts for hydrogen evolution reaction, J Mater Sci, 52 (2017) 7269-7281.
[2] Y. Lin, M. Liu, Y. Pan, J. Zhang, Porous Co–Mo phosphide nanotubes: an efficient electrocatalyst for hydrogen evolution, J Mater Sci, 52 (2017) 10406-10417.
[3] B. Zhang, H. Zhu, M. Zou, X. Liu, H. Yang, M. Zhang, W. Wu, J. Yao, M. Du, Design and fabrication of size-controlled Pt–Au bimetallic alloy nanostructure in carbon nanofibers: a bifunctional material for biosensors and the hydrogen evolution reaction, J Mater Sci, 52 (2017) 8207-8218.
[4] M. Gong, W. Zhou, M.-C. Tsai, J. Zhou, M. Guan, M.-C. Lin, B. Zhang, Y. Hu, D.-Y. Wang, J. Yang, Nanoscale nickel oxide/nickel heterostructures for active hydrogen evolution electrocatalysis, Nature communications, 5 (2014).
[5] M. Li, Peak oil, the rise of China and India, and the global energy crisis, Journal of Contemporary Asia, 37 (2007) 449-471.
[6] X. Yang, et al, Taming the stability of Pd active phases through a compartmentalizing strategy toward nanostructured catalyst supports, Nature Communiations, 10.1 (2019) 1611.
[7] C. Fried, Clean Energy Partnership develops fuel of the future for hydrogen mobility in Germany, Fuel Cells Bulletin, 2011 (2011) 12-14.
[8] A. Ursua, L.M. Gandia, P. Sanchis, Hydrogen production from water electrolysis: current status and future trends, Proceedings of the IEEE, 100 (2012) 410-426.
[9] R. Hashaikeh, B.S. Lalia, V. Kochkodan, N. Hilal, A novel in situ membrane cleaning method using periodic electrolysis, Journal of Membrane Science, 471 (2014) 149-154.
[10] B.S. Lalia, F.E. Ahmed, T. Shah, N. Hilal, R. Hashaikeh, Electrically conductive membranes based on carbon nanostructures for self-cleaning of biofouling, Desalination, 360 (2015) 8-12.

[11] S.F. Anis, R. Hashaikeh, N. Hilal, Functional materials in desalination: A review, Desalination, 468 (2019) 114077.
[12] X. Yan, L. Tian, X. Chen, Crystalline/amorphous Ni/NiO core/shell nanosheets as highly active electrocatalysts for hydrogen evolution reaction, Journal of Power Sources, 300 (2015) 336-343.
[13] H. Zheng, M. Mathe, Hydrogen evolution reaction on single crystal WO 3/C nanoparticles supported on carbon in acid and alkaline solution, International Journal of Hydrogen Energy, 36 (2011) 1960-1964.
[14] S. Zou, J. Liu, H. Kobayashi, C. Chen, P. Qiao, R. Li, L. Xiao, J. Fan, Boosting Hydrogen Evolution Activities by Strong Interfacial Electronic Interaction in ZnO@ Bi (NO3) 3 Core–Shell Structures, The Journal of Physical Chemistry C, 121 (2017) 4343-4351.
[15] Z. Luo, R. Miao, T.D. Huan, I.M. Mosa, A.S. Poyraz, W. Zhong, J.E. Cloud, D.A. Kriz, S. Thanneeru, J. He, Mesoporous MoO3–x Material as an Efficient Electrocatalyst for Hydrogen Evolution Reactions, Advanced Energy Materials, 6 (2016).
[16] S.F. Anis, A. Khalil, G. Singaravel, R. Hashaikeh, A review on the fabrication of zeolite and mesoporous inorganic nanofibers formation for catalytic applications, Microporous and Mesoporous Materials, 236 (2016) 176-192.
[17] S.F. Anis, G. Singaravel, R. Hashaikeh, Electropsun Ni-W/zeolite composite fibers for n-heptane hydrocracking and hydroisomerization, Materials Chemistry and Physics, 200 (2017) 146-154.
[18] S.F. Anis, R. Hashaikeh, N. Hilal, Reverse osmosis pretreatment technologies and future trends: A comprehensive review, Desalination, 452 (2019) 159-195.
[19] J.-y. Leng, X.-j. Xu, N. Lv, H.-t. Fan, T. Zhang, Synthesis and gas-sensing characteristics of WO3 nanofibers via electrospinning, Journal of Colloid and Interface Science, 356 (2011) 54-57.
[20] X.W. Kong, R.L. Zhang, S.K. Zhong, L. Wu, Electrospinning synthesis of 3D porous NiO nanorods as anode material for lithium-ion batteries, Materials Science-Poland, 34 (2016) 227-232.
[21] K. Tang, X. Mu, P.A. van Aken, Y. Yu, J. Maier, "Nano-pearl-string" TiNb2O7 as anodes for rechargeable lithium batteries, Advanced Energy Materials, 3 (2013) 49-53.
[22] E. Formo, E. Lee, D. Campbell, Y. Xia, Functionalization of electrospun TiO2 nanofibers with Pt nanoparticles and nanowires for catalytic applications, Nano Letters, 8 (2008) 668-672.
[23] Y. Yang, L. Xu, C. Su, J. Che, W. Sun, H. Gao, Electrospun ZnO/Bi2O3 nanofibers with enhanced photocatalytic activity, Journal of Nanomaterials, 2014 (2014).
[24] K. Wang, D. Xi, C. Zhou, Z. Shi, H. Xia, G. Liu, G. Qiao, CoSe 2 necklace-like nanowires supported by carbon fiber paper: a 3D integrated electrode for the hydrogen evolution reaction, Journal of Materials Chemistry A, 3 (2015) 9415-9420.
[25] F. Chekin, S. Bagherib, S.B.A. Hamidb, Synthesis of Tungsten Oxide Nanorods by the Controlling Precipitation Reaction: Application for Hydrogen Evolution Reaction on a WO3 Nanorods/Carbon Nanotubes Composite Film Modified Electrode, J. Chin. Chem. Soc, 60 (2013) 447-451.
[26] B.S. Lalia, A. Khalil, T. Shah, R. Hashaikeh, Flexible carbon nanostructures with electrospun nickel oxide as a lithium-ion battery anode, Ionics, 21 (2015) 2755-2762.
[27] B.S. Lalia, T. Shah, R. Hashaikeh, Microbundles of carbon nanostructures as binder free highly conductive matrix for LiFePO4 battery cathode, Journal of Power Sources, 278 (2015) 314-319.
[28] J. Moon, J.-A. Park, S.-J. Lee, S.C. Lim, T. Zyung, Structure and electrical properties of electrospun ZnO–NiO mixed oxide nanofibers, Current Applied Physics, 9 (2009) S213-S216.
[29] P. Frontera, L.A. Scarpino, C. Busacca, P.L. Antonucci, S. Siracusano, A.S. Aricò, High surface area Ti-based mixed oxides nanofibers prepared by electrospinning, Materials Letters, 134 (2014) 281-285.
[30] V. Nair, F. Regius, A. Ragavendar, S. Suman, Role of electrospun ZnO-NiO metaloxide nanocomposite fibers for sensor applications, in: Industrial Engineering and Operations Management (IEOM), 2015 International Conference on, 2015, pp. 1-8.
[31] K. Asokan, J.Y. Park, S.-W. Choi, S.S. Kim, Nanocomposite ZnO–SnO 2 nanofibers synthesized by electrospinning method, Nanoscale research letters, 5 (2010) 747.

[32] C. Wu, C. Li, B. Yang, S. Zhou, D. Shi, Y. Wang, G. Yang, J. He, Y. Shan, Electrospun MnCo2O4 nanofibers for efficient hydrogen evolution reaction, Materials Research Express, 3 (2016) 095018.
[33] Y.H. Li, P.F. Liu, L.F. Pan, H.F. Wang, Z.Z. Yang, L.R. Zheng, P. Hu, H.J. Zhao, L. Gu, H.G. Yang, Local atomic structure modulations activate metal oxide as electrocatalyst for hydrogen evolution in acidic water, Nature communications, 6 (2015) 6:8064.
[34] J. Al-Sharab, R. Sadangi, V. Shukla, S. Tse, B. Kear, Synthesis of Nanostructured Tungsten Oxide (WO2. 9) Fibers and Discs, Crystal Growth & Design, 9 (2009) 4680-4684.
[35] F. Xu, S.D. Tse, J.F. Al-Sharab, B.H. Kear, Flame synthesis of aligned tungsten oxide nanowires, Applied physics letters, 88 (2006) 243115.
[36] T.K. Shah, H.C. Malecki, R.R. Basantkumar, H. Liu, C.A. Fleischer, J.J. Sedlak, J.M. Patel, W.P. Burgess, J.M. Goldfinger, Carbon nanostructures and methods of making the same, U.S. Patent Application No. 14/035,856., in, Google Patents, 2014.
[37] S.F. Anis, R. Hashaikeh, Electrospun zeolite-Y fibers: Fabrication and morphology analysis, Microporous and Mesoporous Materials, 233 (2016) 78-86.
[38] P.C.K. Vesborg, B. Seger, I. Chorkendorff, Recent Development in Hydrogen Evolution Reaction Catalysts and Their Practical Implementation, The Journal of Physical Chemistry Letters, 6 (2015) 951-957.
[39] H. Rietveld, A profile refinement method for nuclear and magnetic structures, Journal of applied Crystallography, 2 (1969) 65-71.
[40] V. Pierre, Pearson's crystal data, crystal structure database for inorganic conpounds (on CD-ROM), (2010).
[41] B. Predel, O-W (Oxygen-Tungsten), in: O. Madelung (Ed.) Ni-Np – Pt-Zr, Springer Berlin Heidelberg, Berlin, Heidelberg, 1998, pp. 1-6.
[42] S.F. Anis, B.S. Lalia, G. Palmisano, R. Hashaikeh, Photoelectrochemical activity of electrospun WO3/NiWO4 nanofibers under visible light irradiation, J Mater Sci, (2017).
[43] E. Kemppainen, A. Bodin, B. Sebok, T. Pedersen, B. Seger, B. Mei, D. Bae, P.C.K. Vesborg, J. Halme, O. Hansen, P.D. Lund, I. Chorkendorff, Scalability and feasibility of photoelectrochemical H2 evolution: the ultimate limit of Pt nanoparticle as an HER catalyst, Energy & Environmental Science, 8 (2015) 2991-2999.
[44] Y.H. Chang, C.T. Lin, T.Y. Chen, C.L. Hsu, Y.H. Lee, W. Zhang, K.H. Wei, L.J. Li, Highly Efficient Electrocatalytic Hydrogen Production by MoSx Grown on Graphene-Protected 3D Ni Foams, Advanced materials, 25 (2013) 756-760.
[45] D.Y. Chung, S.W. Jun, G. Yoon, H. Kim, J.M. Yoo, K.-S. Lee, T. Kim, H. Shin, A.K. Sinha, S.G. Kwon, K. Kang, T. Hyeon, Y.-E. Sung, Large-Scale Synthesis of Carbon-Shell-Coated FeP Nanoparticles for Robust Hydrogen Evolution Reaction Electrocatalyst, Journal of the American Chemical Society, 139 (2017) 6669-6674.
[46] P. Jiang, Q. Liu, Y. Liang, J. Tian, A.M. Asiri, X. Sun, A Cost-Effective 3D Hydrogen Evolution Cathode with High Catalytic Activity: FeP Nanowire Array as the Active Phase, Angewandte Chemie International Edition, 53 (2014) 12855-12859.
[47] J. Tian, Q. Liu, A.M. Asiri, X. Sun, Self-supported nanoporous cobalt phosphide nanowire arrays: an efficient 3D hydrogen-evolving cathode over the wide range of pH 0–14, Journal of the American Chemical Society, 136 (2014) 7587-7590.